DOI: 10.61782/fa.2025.0773

FORUM ACUSTICUM
EURONOISE 2025

SIMULATION METHOD FOR SHOEBOX-SHAPED ROOMS WITH ABSORBING CEILINGS

U. Peter Svensson
Dept. of Electronic Systems,
NTNU, Trondheim, Norway

Kristian H. Reigstad
Dept. of Electronic Systems,
NTNU, Trondheim, Norway

Magne Skålevik
Brekke & Strand AS,
Oslo, Norway

ABSTRACT

A shoebox-shaped room with an absorbing ceiling, and otherwise rigid surfaces, is a common but hard case in room acoustics. Geometrical acoustics fails to predict the low-frequency effects and often also the high-frequency flutter echo effects in such rooms.

Here, the ”surface impedance” method [1] is used, employing the modal solution for a shoebox-shaped room. The absorbing ceiling can be represented by a set of secondary sources, and their vibration velocities are dictated by a matrix equation, where one has the choice to describe the absorber as a locally-reacting material or as an extended-reaction material. The final solution is a sum of the primary source and the secondary source contributions. The frequency-domain formulation is furthermore used to generate band-pass filtered impulse responses, which reveal the temporal decay shape.

In this study, horizontal or vertical modes are excited by using sets of primary monopoles sources. Results demonstrate that a ceiling with an idealized frequency-independent, locally reacting absorber gives a strongly frequency-dependent reverberation time for horizontal modes. Results are compared with reference results calculated with the finite element method.

Keywords: *reverberation, absorption, modal solution, secondary sources*

**Corresponding author*: peter.svensson@ntnu.no.

1. INTRODUCTION

A common case in room acoustics is a shoebox-shaped room with an absorbing ceiling. Well-known challenges with such rooms include flutter echoes and the related highly frequency-dependent reverberation times, and this seemingly simple case can be a hard case [2], [3]. Commonly, sound fields in rooms are analyzed with geometrical acoustics (GA) based methods for the mid- to high-frequency range, and with analytical or numerical methods for low frequencies. The shoebox-shape is the most common room shape which is also practical since analytical solutions exist for rooms with small amounts of damping [4]. In practice, absorbing ceilings can not offer much damping for very low frequencies so the analytical solutions can be useful to predict the first few room modes. However, for more effective absorbers and/or higher frequencies, the situation requires much more complex analytical methods [4], or numerical methods such as finite elements [5] or finite differences [6]. Here we employ a simpler approach where secondary sources are introduced to represent the absorbing ceiling. The amplitudes of the secondary sources are then adjusted so that they, together with the primary source, fulfill the boundary condition at the surface of the absorbers. A few practical aspects with this approach include (1) transfer functions inside the room are calculated with the rigid-wall solution, which is readily available, and (2) the absorber can be modeled as a locally reacting material or an extended-reaction material, via a transfer function matrix for the interaction on the absorber side of the secondary sources. This approach has been used in room acoustics, [7], [4], [8], as well as studies of head-related transfer functions, [9], for single secondary sources. For larger areas, the ”surface impedance method”, [1], can be used to connect shoebox-shaped subdomains or, like here, model absorbing surfaces.

2. THEORY

2.1 The modal solution in a shoebox-shaped room

The sound pressure at a point $\boldsymbol{x}$ in a shoebox-shaped room with a small amount of losses, as caused by a point source, the "primary source", at point $\boldsymbol{x}_\mathrm{P}$, with a volume velocity U_P, is given by, [4],

$$p(\boldsymbol{x}) = U_\mathrm{P} \frac{\mathrm{j}\omega\rho_0 c^2}{V} \sum_\mathrm{N} A_\mathrm{N} \frac{\psi_\mathrm{N}(\boldsymbol{x})\psi_\mathrm{N}(\boldsymbol{x}_\mathrm{P})}{\omega_\mathrm{N}^2 - \omega^2 + 2j\delta_\mathrm{N}\omega_\mathrm{N}} \tag{1}$$

where a time-harmonic factor $\mathrm{e}^{\mathrm{j}\omega t}$, has been suppressed, and N is an abbreviation for the integer triplet that represents the mode number, $\mathrm{N} = (n_x, n_y, n_z)$ where $n_i \in [0, 1, 2, ...]$. Furthermore, the mode scale factor, A_N, is 2/4/8 if, respectively, one, two, or all three integers, n_i, are non-zero. The eigenfunctions are given by

$$\psi_\mathrm{N}(\boldsymbol{x}) = \cos\frac{n_x\pi x}{L}\cos\frac{n_y\pi y}{W}\cos\frac{n_z\pi z}{H} \tag{2}$$

where the rooms dimensions in the x, y, and z directions are L, W, H, see Fig. 1. The mode resonance angular frequencies are

$$\omega_\mathrm{N} = \pi c\sqrt{\left(\frac{n_x}{L}\right)^2 + \left(\frac{n_y}{W}\right)^2 + \left(\frac{n_z}{H}\right)^2} \tag{3}$$

and each mode has a decay constant, δ_N, which is related to the reverberation time as $\delta_\mathrm{N} = 3\ln 10/T_{60}$. The expression in Eq. (1) assumes a single monopole source but superposing many monopoles is straightforward. Thus, by placing a line of monopoles along the y-coordinate, all modes with $n_y > 0$ can be suppressed. Likewise, by distributing monopoles across the plane $x = 0$, only modes with $n_y = 0, n_z = 0, n_x \geq 0$ will be excited, that is, horizontal modes.

The sum in Eq. (1) is converging quite slowly, but can be computed somewhat more efficiently with techniques such as Cesaro summation, [10], for the higher-order modes.

2.2 Introducing secondary sources

In addition to the primary monopole source used above, secondary sources in the form of rectangular pistons are introduced, at $z = H$. For such a source with vibration velocity v_S and area S_S, extending such that $x_\mathrm{S} \in [x_1, x_2], y_\mathrm{S} \in [y_1, y_2]$, Eq. (1) is modified into, [11],

$$p(\boldsymbol{x}) = v_\mathrm{S} \frac{\mathrm{j}\omega\rho_0 c^2}{V} \sum_\mathrm{N} A_\mathrm{N} \frac{\psi_\mathrm{N}(\boldsymbol{x})}{\omega_\mathrm{N}^2 - \omega^2 + 2j\delta_\mathrm{N}\omega_\mathrm{N}}$$
$$\cdot \frac{LW}{\pi^2} \frac{\sin\frac{n_x\pi x_2}{L} - \sin\frac{n_x\pi x_1}{L}}{n_x}$$
$$\cdot \frac{\sin\frac{n_y\pi y_2}{W} - \sin\frac{n_y\pi y_1}{W}}{n_y} \cos(n_z\pi). \tag{4}$$

The expression in Eq. (1) is used to define a primary source transfer function (TF), $H(\boldsymbol{x} \leftarrow \boldsymbol{x}_\mathrm{P}) \coloneqq p(\boldsymbol{x})/U_\mathrm{P}$. Another TF definition is used for the secondary sources, $G(\boldsymbol{x} \leftarrow \boldsymbol{x}_\mathrm{S}) \coloneqq p(\boldsymbol{x})/v_\mathrm{S}$, and there will be two different G TFs, one for the room side of the secondary sources, and another one for the absorber side of the secondary sources, as explained further below. Secondary piston sources are placed at the location of the absorber as indicated in Fig. 1, and the sound pressure at position $\boldsymbol{x}$ is then a sum of the contributions by the primary and secondary sources,

$$p(\boldsymbol{x}) = U_\mathrm{P} H(\boldsymbol{x} \leftarrow \boldsymbol{x}_\mathrm{P}) - \sum_{i=1}^{N_\mathrm{S}} v_{\mathrm{S}i} G(\boldsymbol{x} \leftarrow \boldsymbol{x}_\mathrm{S}) \tag{5}$$

where the negative sign of the secondary source contributions is caused by the definition of positive v_S in the direction out of the room, see Fig. 1.

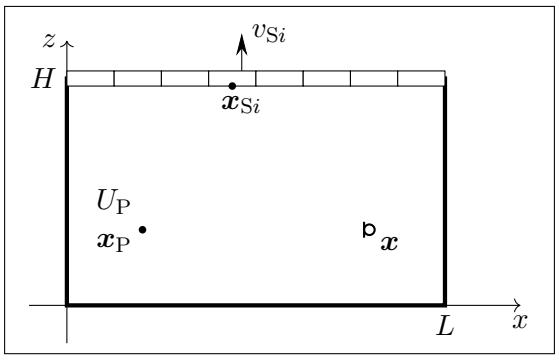

Figure 1. The xz-projection of a shoebox-shaped room. A primary source at $\boldsymbol{x}_\mathrm{P}$ and a number of secondary pistons sources at $\boldsymbol{x}_{\mathrm{S},i}$ are marked.

The velocities of the N_S secondary sources can be found from solving a matrix equation

$$(\mathbf{G}_\mathrm{room} + \mathbf{G}_\mathrm{abs.})\,\mathbf{v}_\mathrm{S} = \mathbf{p}_\mathrm{S} \tag{6}$$

where $\mathbf{v}_\mathrm{S} \in \mathbb{C}^{N_\mathrm{S}\times 1}$ is an array of the unknown secondary source velocities, $\mathbf{p}_\mathrm{S} \in \mathbb{C}^{N_\mathrm{S}\times 1}$ is an array of the sound pressure amplitudes at the secondary source positions, when these are considered rigid, as caused by the

primary source, so the pressure can be represented by the TFs for the rigid room,

$$\mathbf{p}_{\mathrm{S}} = U_{\mathrm{P}}\left[H(\boldsymbol{x}_{\mathrm{S},i} \leftarrow \boldsymbol{x}_{\mathrm{P}})\right]$$

Furthermore, the TF matrix $\mathbf{G}_{\mathrm{room}} \in \mathbb{C}^{N_{\mathrm{S}} \times N_{\mathrm{S}}}$ contains all TFs between secondary sources, also computed for the room with rigid walls. The TF matrix which represents the absorber, $\mathbf{G}_{\mathrm{abs.}} \in \mathbb{C}^{N_{\mathrm{S}} \times N_{\mathrm{S}}}$, will for a locally reacting material have non-zero values, the specific acoustic impedance values, only along the diagonal. For an extended reaction material, the TFs $G_{\mathrm{abs.}}(\boldsymbol{x}_{\mathrm{S},i} \leftarrow \boldsymbol{x}_{\mathrm{S},j})$ must correctly model the propagation inside the absorber, for a situation where the secondary source surface is rigid, and a single piston source is radiating sound into the absorber.

2.3 Reference solution - 2D finite element calculations

The software COMSOL Multiphysics, version 6.0, was used to compute reference results, [12]. The room was simulated as a 2D case, meshing the room with triangular elements to give at least five elements per wavelength at 2000 Hz, leading to 27562 triangular elements. In order to mimic the modal solution with small losses, Helmholtz equation was modified by including atmospheric absorption and an air attenuation coefficient of 0.004004 Np/m, which gave a reverberation time around 5 seconds for the empty room, for all frequencies.

2.4 Determining the T_{60}-value.

When the mode-suppressing technique described above is used, it is possible to get well separated resonance peaks in the TFs. Then the bandwidth, $\Delta\omega$, of each resonance peak can be determined and

$$T_{60} = \frac{6 \ln 10}{\Delta\omega} \tag{7}$$

where $\Delta\omega$ is the angular bandwidth of the resonance, that is, the distance in angular frequency between two points of the curve $|H(\omega)|$ around a resonance frequency, ω_0, where $|H(\omega)| = |H(\omega_0)|/\sqrt{2}$. This estimate of T_{60} is assuming that the decay is exponential, but it can not be checked if the assumption is true without analyzing the shape of the frequency response around the peak.

2.5 Constructing impulse responses

In addition to the frequency-domain (FD) results described above, impulse responses (IRs) were generated. This was done by choosing a target sampling frequency, f_{S}, and FFT-size, n_{FFT}. Here, f_{S} = 4 kHz and n_{FFT} = 16384 were chosen, which generated IRs of length $\approx$ 4.1 s. FD results were then computed for a range of frequencies with the frequency step $\Delta f = f_{\mathrm{S}}/n_{\mathrm{FFT}} \approx 0.24$ Hz. The third-octave bands from 63 Hz to 1 kHz were chosen, and the computed frequency range was a factor 1.3 beyond the edges of the third-octave bands, that is from 44.7 Hz to 1412.5 Hz, a total of 7381 frequencies. The FD results were set to zero for the rest of the required frequency range: from 0 Hz to 44.7 Hz, and from 1412.5 Hz to 2000 Hz, to fill a vector of 8193 FD values. The 8191 values above $f_{\mathrm{S}}/2$ were complex-conjugated, mirrored copies of the computed ones, and an inverse FFT then yielded a real-valued IR which was subsequently filtered so that T_{20} and T_{30}-values could be determined via backward integration for each third-ocatve band. Backwards filtering was used since the lowest bands had very short reverberation times in some cases. By comparing T_{20} and T_{30} values, signs of non-exponential decays could be detected.

3. NUMERICAL EXAMPLES

A room of dimensions (L, W, H) = (5 m, 4 m, 2.6 m) was studied, with the entire ceiling covered with an absorbing material which was modeled as locally reacting, and with frequency-independent impedance values of $Z_{\mathrm{s,abs.}} = (2, 3, 5, 7, 10)\rho_0 c$. These idealized values would be difficult to achieve in practice, in particular for low frequencies, but are useful in simulations. A set of 120 secondary sources in the form of pistons was placed at the ceiling surface, which implies 7 elements per wavelength at 1180 Hz, the highest frequency studied in the FD simulations. The pistons extended across the y-direction (the W-direction).

In order to excite only horizontal modes in the x-direction (the L-direction), the entire wall of the room, at $x = 0$, was used as a primary source, with the vibration velocity 1 m/s. In the modal summation, Eq. (4), modes with resonance frequencies up to twice the highest frequency of interest were included. The rigid-walled room was given a δ-value in Eq. (1) which corresponded to $T_{60} = 5$ s. Since primary sources and secondary sources extended across the entire y-dimension, only mode numbers with $n_y = 0$ were included in Eq. (4).

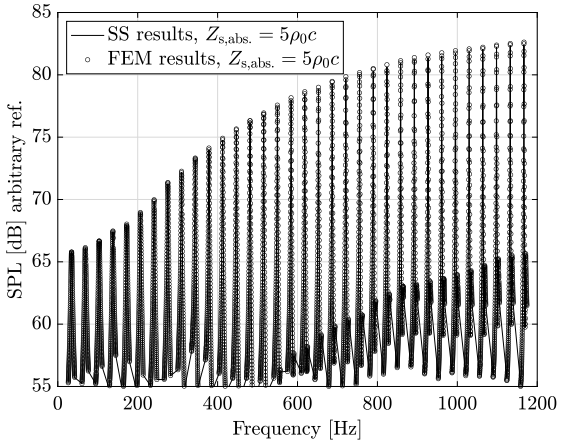

Figure 2. The frequency response in the modeled room, when the end-wall ($x = 0$) acts as a piston primary source and thus excites only modes in the length direction in the room. The ceiling had 120 secondary piston sources which fulfilled the locally reacting impedance of 5 $\rho_0 c$.

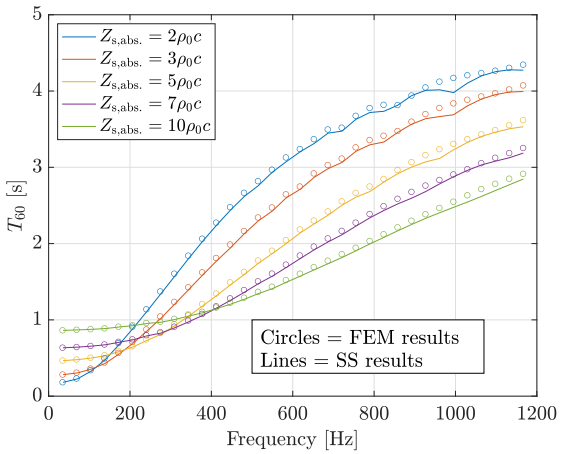

Figure 3. Resulting reverberation times from analyzing each resonance peak in frequency response curves like those in Fig. 2, for five different values of ceiling absorber impedance, $Z_{s,abs.}$, for horizontal-mode excitation.

4. RESULTS AND DISCUSSION

As one result example, Fig. 2 shows the frequency response up to 1180 Hz as computed with the SS method and with COMSOL Multiphysics ("FEM results"), for the ceiling impedance $Z_{s,abs.} = 5\rho_0 c$. Note that the frequency response was not computed for the entire frequency ranges between the resonance peaks. The excitation of the room with the entire end-wall as a piston explains the constant distribution of resonance frequencies. The resonance peak values were systematically lower with the SS method, starting at 0.02 dB lower at 34 Hz, increasing roughly linearly to 0.2 dB lower at 500 Hz. Above 500 Hz a very small shift in resonance frequency could be observed as well, increasing to 0.1 Hz at 1200 Hz. The resonance peaks were then analyzed to estimate the reverberation time values, as given by Eq. (7). The reverberation times for the five different impedance values listed above are plotted in Fig. 3. The SS results are consistently lower than the FEM results, by an amount increasing roughly linearly from 0 s up to 0.05 s at 800 Hz, and then fluctuating between 0.19 s and 0 s above 800 Hz. These deviations for the T_{60}-values are considered as small enough that the results seem to confirm that the SS method is valid.

It is clear that the ceiling absorber has much effect on the horizontally excited sound field at low frequencies, but less and less so as the frequency is increased. This observation is also reflected in the relative change in T60 which is substantially higher below ca 150 Hz than for higher frequencies. At the low-frequency end, where the sound pressure is almost constant across the room, it doesn't matter where absorption material is placed and thus the absorber can be highly effective. As the frequency is increased, the flutter echo phenomenon becomes more and more prominent which means that the ceiling absorber has less and less influence on the horizontally propagating sound waves. Thus, as frequency is increased, a transition occurs between two very different T_{60}-values. This observation can be compared with the model developed in [13] for rooms with absorbing ceilings, where the diffuse sound field model is developed into a two-component sound field: a diffuse part, and one part with grazing-incidence, i.e., horizontally propagating sound waves. That model assigns a much longer reverberation time to the grazing-incidence components, as observed here, but also applies a volume scattering coefficient. A high value of such a volme scattering coefficient can make the ceiling absorber effective also for the grazing incidence-component. The model presented here has no such scattering effect.

At the lowest frequencies, the absorber with the lowest impedance, $2\rho_0 c$, leads to the lowest reverberation time, which seems intuitively correct. However, above

200-300 Hz, a surprising effect can be observed: the absorber with the lowest impedance gives a longer reverberation time, which seems counterintuitive. The two calculation methods do agree, so we draw the conclusion that this effect will happen - if we have truly locally reacting absorber materials. For even higher impedance values than $10\rho_0 c$, results for which are not shown here, the reverberation time will start to increase, so the lowest T_{60}-values in the frequency range 600 Hz - 1.1 kHz seem to occur for the impedance value $Z_{\mathrm{s,abs.}} \approx 12\rho_0 c - 24\rho_0 c$. The very effective absorption at low frequencies might seem surprising in this case where horizontally propagating sound waves are excited, since the absorption coefficient usually is shown to tend to zero for grazing incidence, [4]. However, that vanishing absorption coefficient is for a single infinite absorption surface. In an enclosed space, a wave propagating along an impedance surface will be highly affected since the grazing wave front will necessarily generate a particle velocity component into the impedance surface.

An example of an impulse response generated as described in Section 2.4 is shown in Fig. 4, for the ceiling absorber impedance $Z_{\mathrm{s,abs.}} = 5\rho_0 c$, also for horizontal mode excitation. Such impulse responses were then filtered in third-octave bands, from 63 Hz to 1 kHz (excluding the 80 Hz band where there was no resonance peak). The T_{20} and T_{30} values were computed for the same five impedance values as in Fig. 3, and the T_{30}-values from the generated IRs are shown in Fig. 5, together with the T_{60}-results from the frequency-domain analysis, as were presented in Fig. 3. There is a small systematic difference between the FD-results and those from the IR analysis which can partly be explained by that from the 250 Hz band, there will be at least two resonance peaks in each band, and those two resonance peaks will have slightly different T_{60}-values, as can be seen in Fig. 3 (two consecutive data points always have slightly different T_{60}-values). Furthermore, the FD results in Fig. 3 are plotted at the exact resonance frequencies, whereas the values for the IR-analysis are plotted at the band centre frequencies, and this will give a systematic shift in the frequency direction. The T_{20}-values were found to be within $-0.9\%, +0.2\%$ of the T_{30}-values, for the five tested ceiling absorber impedance values, and for all the frequency bands tested. These small differences do not indicate any non-exponential decays.

Since the SS method seem to be verified, it can be used further to investigate the influence of the room height. It could also be investigated if moving some absorbers to the sidewalls would reduce the flutter echo effect. Furthermore, some extended-reaction material model can be explored, and more realistic, frequency-dependent impedance values should be used. Extended-reaction material models have been shown to give absorption properties that are closer to measurements than local-reaction models [13], [14].

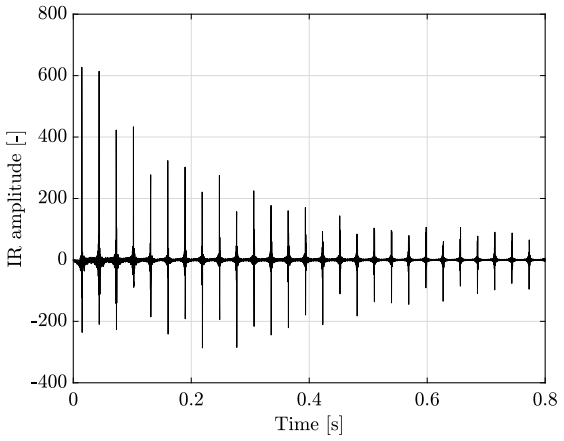

Figure 4. An example of an impulse response generated as described in Section 2.4, for the ceiling absorber impedance, $Z_{\mathrm{s,abs.}} = 5\rho_0 c$, and horizontal-mode excitation.

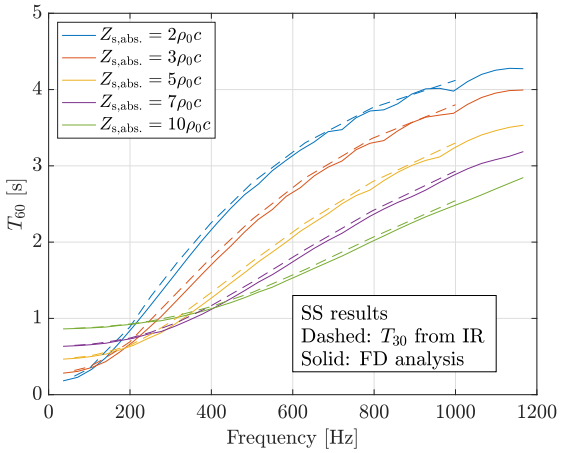

Figure 5. T_{60}-results for horizontal-mode excitation, both from IR analysis (T_{30}-results) and from FD analysis (same results as in Fig. 3).

.

5. CONCLUSIONS

The presented numerical simulation model for a shoebox-shaped room with an absorbing ceiling seems to be validated by the comparison with reference results by the finite element method. This verification was only done for 2D-cases but there is no reason to believe that the method would not work equally well for 3D-cases.

As regards the sound field, a ceiling absorber can be highly effective at low frequencies, if its impedance is suitable. Without scattering in a room, ceiling absorbers are increasingly ineffective as frequency is increased, gradually leading to more and more prominent flutter echos. An unexpected effect is that in a mid-frequency range, the lowest impedance does not necessarily give the lowest reverberation time.

6. REFERENCES

[1] G. Pavic., L. Du. Modelling of multi-connected acoustical spaces by the surface impedance approach. In *Proc. of INTER-NOISE 2016*, pages 4278–4286, Hamburg, Germany, 2016.

[2] M. Skålevik. Small room acoustics – The hard case. In *Proc. of Forum Acusticum 2011*, 27 June-1 July, Aalborg, Denmark, 2011.

[3] M. Skålevik. How much scattering is sufficient to soften the Hard Case?. In *Proc. of Forum Acusticum 2014* , 7-12 September, Krakow, Poland, 2014.

[4] H. Kuttruff. *Room acoustics, 4th ed.*. Spon press, London, UK, 2000.

[5] F. Pind, C.-H. Jeong, A. P. Engsig-Karup, J. S. Hesthaven, and J. Strømann-Andersen. Time domain room acoustic simulations with extended-reacting porous absorbers using the discontinuous Galerkin method. *J Acoust Soc Am*, 148:2851–2863, 2020.

[6] B. Hamilton, S. Bilbao. FDTD Methods for 3-D room acoustics simulation with high-order accuracy in space and time. *IEEE Trans Audio Speech Lang Proc*, 25:2112–2124, 2017.

[7] C. Zwikker, C. W. Kosten. *Sound absorbing materials*. Elsevier, New York, USA, 1949.

[8] P. Sjösten, U. P. Svensson, B. Kolbrek, K. B. Evensen. The effect of Helmholtz resonators on the acoustic room response. In *Proc. of BNAM 2016*, 20-22 June, Stockholm, Sweden, 2016.

[9] H. Møller. Fundamentals of binaural technology. *Appl Acoust*, 36:171–218, 1992.

[10] E. C. Titchmarsh. *The theory of functions, Second edition*. Oxford University Press, Oxford, UK, 1939.

[11] B. Kolbrek. *Extensions to the mode matching method for horn loudspeaker simulation*. PhD thesis, NTNU, Trondheim, Norway, 2016.

[12] COMSOL AB. *COMSOL Multiphysics® reference manual*. Retrieved from `https://doc.comsol.com/6.3/docserver/#!/com.comsol.help.comsol/html_COMSOL_ReferenceManual.html`, 2025.

[13] E. Nilsson, E. Arvidsson. An energy model for the calculation of room acoustic parameters in rectangular rooms with absorbent ceilings. *Appl Sci*, 11:6607, 2021.

[14] C.-H. Jeong. Guideline for adopting the local reaction assumption for porous absorbers in terms of random incidence absorption coefficients. *Acta Acustica united w Acustica*, 97:779–790, 2011.